PIER C

(Received 8 January 2026, Accepted 2 February 2026, Scheduled 15 April 2026texpreamble(xxx);)

A Novel Compact Ultra-Wideband Vivaldi Antenna with Concentric Arc Patches and Elliptical Slots

Yi Si[1,2], Pengju Yang[1,2,*], Rui Wu[1,3], and Linzi Wang[1,2]

[1]*School of Physics and Electronic Information, Yan'an University, Yan'an 716000, China*
[2]*Shaanxi Key Laboratory of Intelligent Processing for Big Energy Data, Yan'an University, Yan'an 716000, China*
[3]*School of Integrated Circuits and Electronics, Beijing Institute of Technology, Beijing 100081, China*

ABSTRACT: To meet the requirements of antenna miniaturization and wide impedance bandwidth in ultra-wideband (UWB) systems, a novel compact UWB Vivaldi antenna is presented in this work. Based on the conventional planar Vivaldi configuration, the radiating arms are etched with elliptical slots, and the front end of the tapered slot is loaded with concentric arc parasitic patches to regulate the surface current distribution and enhance broadband impedance matching. Simulated and measured results demonstrate that the presented antenna achieves a reflection coefficient below -10 dB over the frequency range of 6.61–1.06 GHz, corresponding to a relative bandwidth of 104.45%, with a compact size of $14.5\times19.8\times0.51$ mm^3, while maintaining a single-layer planar structure without increasing structural complexity. It is also indicated that stable end-fire radiation characteristics and low cross-polarization levels are maintained at several representative frequencies. The presented design simultaneously realizes significant size reduction and ultra-wide impedance bandwidth, providing a simple and practical solution for compact UWB Vivaldi antenna applications.

1. INTRODUCTION

With the widespread application of UWB technology in wireless communications, radar sensing, nondestructive testing, and imaging systems, antennas are required to simultaneously provide a wide impedance bandwidth and a compact physical size. The Vivaldi antenna, first presented by Gibson in 1979 [1], is a typical broadband traveling-wave antenna that has been widely employed in UWB systems due to its wide operating bandwidth, good directivity, and ease of planar implementation. However, conventional Vivaldi antennas generally rely on a relatively large tapered aperture to support efficient radiation at low frequencies. While enabling UWB performance, this characteristic often results in large antenna dimensions, limiting their application in compact and highly integrated systems [2].

To address these limitations, various miniaturization and bandwidth-enhancement techniques for Vivaldi antennas have been reported. These methods mainly focus on extending the effective electrical length and regulating the radiation modes. Structural perturbations introduced into radiating arms or tapered-slot regions, such as serrated edges and nonuniform slots, can effectively elongate the surface current path and improve low-frequency impedance matching, thereby broadening the operating bandwidth within a limited physical size [3]. In addition, bending or folding the radiating arms enables a longer equivalent current path to be achieved within a constrained space, which helps maintain or even enhance low-frequency radiation performance [4]. Half-mode Vivaldi antennas based on image theory replace one symmetric radiating arm with an electric wall or metallized vias, achieving size reduction while preserving the impedance bandwidth and radiation characteristics [5]. In antipodal Vivaldi antennas, introducing additional exponential strip arms can effectively reduce the lower edge cut-off frequency, thereby achieving antenna miniaturization and improving impedance bandwidth without significantly compromising radiation characteristics [6]. Furthermore, compact Vivaldi antennas incorporating nonuniform slot shaping and dielectric lens loading at the aperture have been shown to enhance radiation directivity and gain stability while extending the impedance bandwidth through additional resonances introduced by extended ground structures [7]. Semi-structured Vivaldi antennas further compress the antenna aperture by equivalently replacing one radiating arm with a ground plane and have been successfully extended to transparent antennas and function-integrated designs [8]. Meanwhile, UWB antipodal Vivaldi antennas incorporating parasitic resonator structures have been developed for microwave head imaging applications, where enhanced gain, improved reflection coefficient, and broadband radiation stability over the 3.1–10 GHz frequency range are essential for reliable biomedical diagnostics [9]. Although recent studies have reported electrically compact Vivaldi antennas with substantial miniaturization and broadband performance, further optimization of structural simplicity, radiation stability, and integration compatibility for practical UWB systems still warrants investigation [10].

In this study, a novel compact UWB Vivaldi antenna is designed and experimentally validated. By employing concentric arc radiating patches and elliptical-slot structures, the presented design simultaneously enhances the impedance bandwidth and

* Corresponding author: Pengju Yang (pjyang@yeah.net).

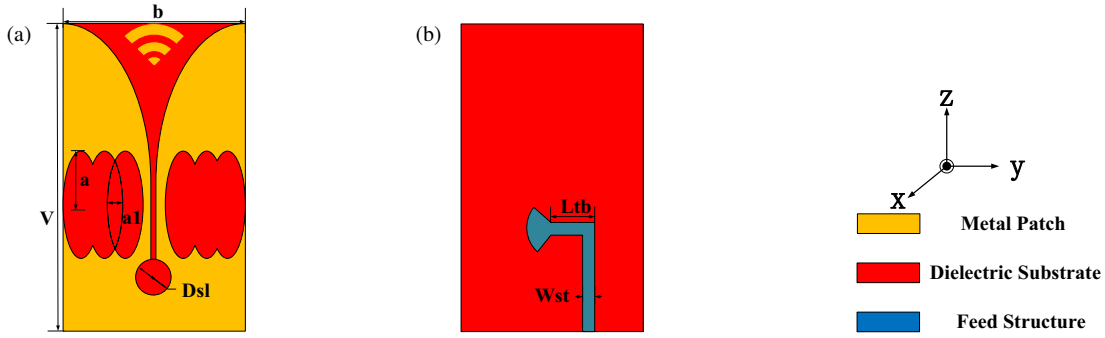

FIGURE 1. The structure of the presented Vivaldi antenna. (a) Front. (b) Back.

gain performance while maintaining the same aperture size as that of a conventional planar Vivaldi antenna. The elliptical slots act as tunable geometric elements, which increase the design flexibility without increasing the structural complexity. Specifically, the overlapping arrangement of these elliptical slots creates a serpentine-like conductive boundary that functions as an efficient slow-wave mechanism. This design effectively elongates the electrical current path within a limited footprint, providing a fundamental mechanism for achieving both extreme miniaturization and ultra-wide impedance bandwidth. This configuration effectively mitigates the gain degradation commonly observed in conventional Vivaldi antennas at both the low and high frequencies. The proposed antenna achieves UWB performance together with compact size, making it suitable for UWB communication, through-wall radar sensing [11–13], and high-resolution imaging applications [14–16].

2. ANTENNA DESIGN

Figure 2 illustrates the three antenna configurations investigated in this work: the original antenna (OA), improved antenna (IA), and presented antenna (PA). OA corresponds to a conventional planar Vivaldi antenna. To improve broadband impedance matching without increasing the antenna aperture, IA introduces cascaded elliptical slots into the radiating arms on both sides of the tapered slot. Technically, these elliptical slots are designed with a specific 1.5 mm overlap ($a1$), forming a serpentine-like conductive boundary along the radiator. This unique configuration acts as an efficient slow-wave mechanism, which forces the surface currents to detour significantly along the undulating perimeters [17]. This geometrical loading effectively extends the equivalent surface-current path and introduces additional broadband resonances, leading to a bandwidth enhancement. Furthermore, based on the IA configuration, the PA loads concentric arc parasitic patches at the front end of the tapered slot while retaining two pairs of elliptical slots. Because of the modified current distribution and the synergistic effect between the overlapping slots and arc patches, the lower cutoff frequency is shifted downward; high-frequency impedance matching is improved; and the end-fire radiation intensity and antenna gain are simultaneously enhanced.

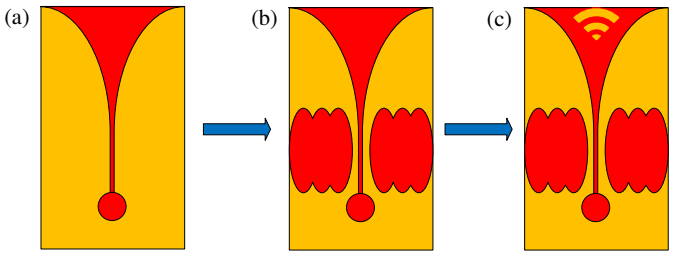

FIGURE 2. Configurations of the three antennas. (a) OA. (b) IA. (c) PA.

The antenna consisted of an upper radiating structure and a lower feeding structure. The substrate was Rogers RO4350 with a relative permittivity of 3.66, loss tangent of 0.004, and thickness of 0.51 mm. A standard 50 Ω excitation port was employed to approximate the practical operating conditions.

The tapered-slot profile of the radiating arms is defined by an exponential curve, as shown in (1). Here, α represents the taper opening rate, which is used to control the expansion speed of the slot and is set to 550 in this work. The constants c_1 and c_2 in (2) and (3) are jointly determined by the coordinates of the starting and ending points of the exponential curve to ensure a smooth transition under the given aperture and length constraints, which is beneficial for broadband traveling-wave radiation. The coordinates of the starting and ending points are $P_1(x_1, y_1) = (0\,\text{mm}, 0.15\,\text{mm})$ and $P_2(x_2, y_2) = (9.9\,\text{mm}, 7.25\,\text{mm})$, respectively.

$$y = c_1 e^{\alpha x} + c_2 \tag{1}$$

$$c_1 = \frac{y_2 - y_1}{e^{\alpha x_2} - e^{\alpha x_1}} \tag{2}$$

$$c_2 = \frac{y_1 e^{\alpha x_2} - y_2 e^{\alpha x_1}}{e^{\alpha x_2} - e^{\alpha x_1}} \tag{3}$$

Based on the design procedure and practical fabrication constraints, joint optimization and full-wave simulations of the geometrical parameters of the antenna are carried out using ANSYS HFSS. The final antenna configuration and the corresponding optimized dimensions are presented in Fig. 1 and Table 1, respectively.

Figure 3 compares the simulated reflection coefficients (S_{11}) of the three antennas, namely OA, IA, and PA. It can be observed that the OA operates over a frequency range of 10.15–18.63 GHz. After introducing the cascaded elliptical slots, the lower cutoff frequency of the IA is shifted downward to 8.95 GHz, while the upper cutoff frequency is extended to

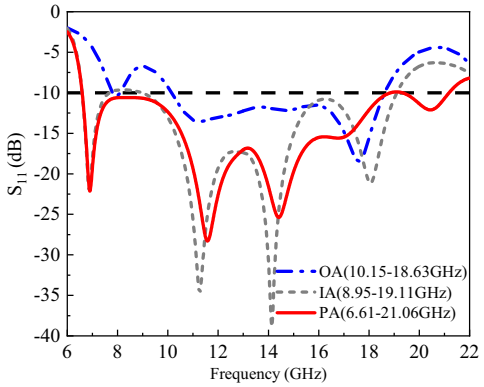

FIGURE 3. Simulated reflection coefficients of the designed antennas.

TABLE 1. Parameters of the presented antenna.

Parameters	Size	Unit	Parameters	Size	Unit
b	14.5	mm	Wst	0.68	mm
Lg	4	mm	Wsl	0.3	mm
Ltc	1.39	mm	p	0.51	mm
Dsl	1.5	mm	v	19.8	mm
La	0.34	mm	$r1$	2.4	mm
Ltb	2.52	mm	a	4.2	mm
$a1$	1.5	mm			

19.11 GHz, indicating that the presented slot structure effectively improves broadband impedance matching. Furthermore, by loading concentric arc parasitic patches at the front end of the tapered slot, the lowest cutoff frequency of the PA was further reduced to 6.61 GHz, and the upper cutoff frequency was increased to 21.06 GHz. Consequently, the operating bandwidth is of the antenna is significantly expanded to 6.61–21.06 GHz, corresponding to a fractional bandwidth of 104.45%.

To further investigate the design principle and ensure the structural robustness of the PA, a parametric sensitivity study was performed on the major axis length a of the elliptical slots and the number n of the concentric arc patches. As shown in Fig. 4, the major axis a primarily determines the lower cutoff frequency. When a is optimized at 4.2 mm, the antenna achieves the widest impedance matching. Increasing or decreasing a leads to a shift in resonance and a degradation of matching in the 8–11 GHz range. Furthermore, Fig. 5 illustrates the effect of the number of arc patches n. It is observed that $n = 3$ provides the best high-frequency stability, particularly above 15 GHz, by regulating the surface current distribution at the aperture. This analysis confirms that the chosen dimensions in Table 1 are optimal for balancing miniaturization and UWB performance.

The surface current distribution of OA is mainly concentrated near the tapered-slot edges of the metallic radiating patch [18]. These currents generate additional radiation outside the main radiation direction, which increases sidelobe levels and degrades the end-fire directivity and the overall gain. Fig. 6 presents the simulated surface current distributions of the OA and PA at 8.5 GHz, 12.5 GHz, and 18.0 GHz. At 8.5 GHz,

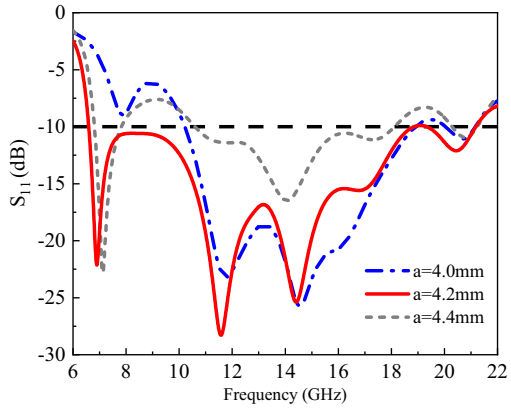

FIGURE 4. Simulated reflection coefficients of the PA for various elliptical slot major axis lengths a.

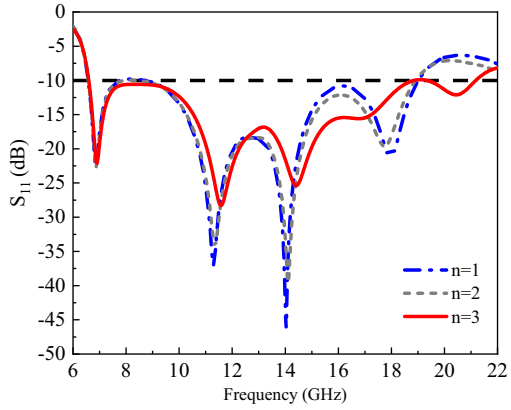

FIGURE 5. Simulated reflection coefficients of the PA for various numbers n of concentric arc patches.

strong current concentrations were observed along the edges of the OA, resulting in pronounced radiation from the lateral sides of the antenna. By contrast, the two pairs of cascaded elliptical slots in the PA, designed with a specific 1.5 mm overlap, force the surface currents to detour along a serpentine-like path. This visual evidence confirms the slow-wave mechanism: the interconnected elliptical boundaries create a more tortuous path for the current compared to the OA, effectively extending the electrical length within a limited footprint. The improved current distribution enabled the PA to operate at lower frequencies, thereby enhancing its low-frequency performance. By optimizing the surface current distribution, the sidelobe radiation is significantly reduced, and the radiation efficiency at low frequencies is improved. At 12.5 GHz, the surface currents captured by the cascaded elliptical slots of the PA are effectively re-coupled to the tapered-slot region, whereas the concentric arc parasitic patches also concentrate a portion of the surface currents, resulting in an extended current path. This synergistic interaction between the overlapping slots and arc patches further optimizes the energy coupling, leading to a noticeable gain improvement, as shown in Fig. 7. At 18.0 GHz, the concentric arc parasitic patches continued to capture surface currents and couple them to the tapered slot, thereby regulating the current distribution and further strengthening the radiation in the main lobe direction.

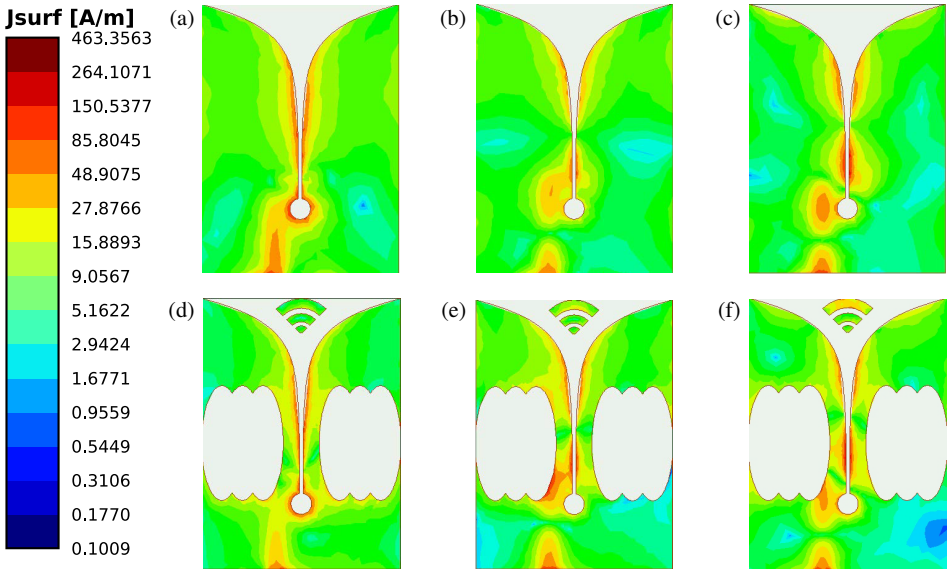

FIGURE 6. Simulated surface current distributions of the OA and PA antennas at different frequencies. (a) OA at 8.5 GHz. (b) OA at 12.5 GHz. (c) OA at 18.0 GHz. (d) PA at 8.5 GHz. (e) PA at 12.5 GHz. (f) PA at 18.0 GHz.

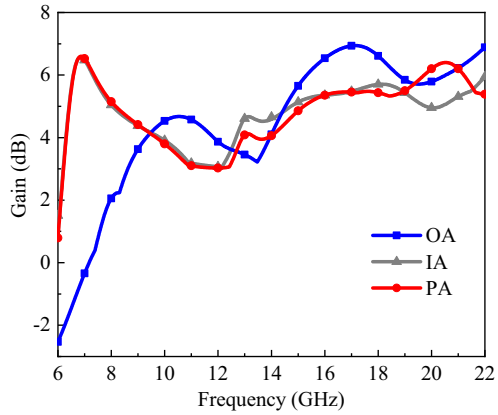

FIGURE 7. Gains of OA, IA, and PA.

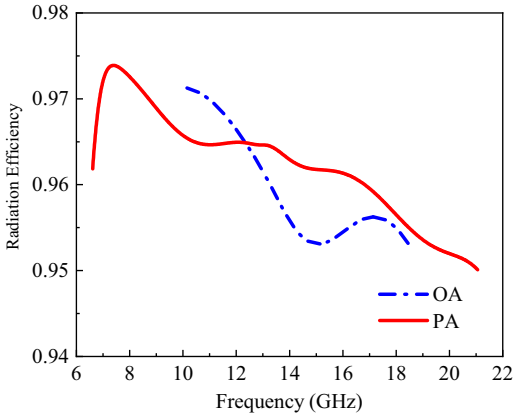

FIGURE 8. Radiation efficiency of OA and PA.

To more clearly illustrate the enhancement in radiation directivity after antenna modification, Fig. 7 presents the simulated gain curves of the OA, IA, and PA configurations. The gain variation of the IA is also included for comparison, because the IA serves as an intermediate structure in the design process. This comparison clearly illustrates the role of each structural modification in the evolution of the performance of the proposed antenna.

The IA effectively improves the overall antenna gain, with the minimum gain increasing from −2.64 dB to 1.04 dB. However, although the low-frequency gain was enhanced, the operating bandwidth was not significantly expanded, and a slight degradation in the high-frequency gain was observed. In contrast, the PA overcomes these limitations by not only increasing the high-frequency gain from 4.95 dB to 6.4 dB, but also extending the operating bandwidth to 6.61–21.06 GHz, thereby addressing the deficiencies of the previous two antenna configurations. To further evaluate the antenna performance during the design process, Table 2 compares the key performance metrics of the three antenna configurations considered in this study, including the operating and fractional bandwidths. Compared with OA and IA, which serve as reference and intermediate structures, respectively, PA exhibits superior performance in terms of the main performance indicators.

The results in Table 2 have already demonstrated the significant expansion of the impedance bandwidth achieved by the proposed PA. As illustrated in Fig. 7, the proposed design also exhibits substantial improvements in gain. To verify that these advancements do not come at the expense of radiation capability, the simulated radiation efficiency was investigated. Fig. 8

TABLE 2. Comparison of operational and relative bandwidths.

	Operational Bandwidth	Relative Bandwidth
OA	10.15–18.63 GHz	58.93%
IA	8.95–19.11 GHz	72.42%
PA	6.61–21.06 GHz	104.45%

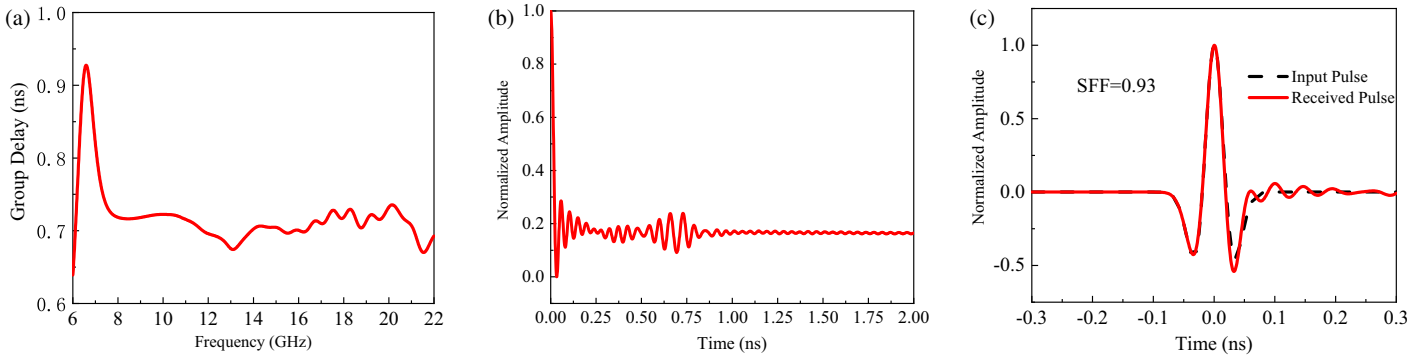

FIGURE 9. Time-domain characteristics of the PA. (a) Group delay. (b) Normalized impulse response. (c) Pulse fidelity comparison.

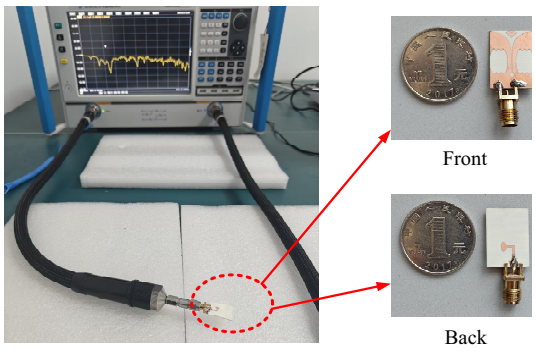

FIGURE 10. Measurement setup and fabricated PA antenna prototype.

illustrates the radiation efficiency of the proposed PA within the operating band from 6.61 GHz to 21.06 GHz, compared with the initial structure within its specific working range from 10.15 GHz to 18.63 GHz. It is observed that the proposed antenna maintains an exceptionally high efficiency, consistently exceeding 95.0% throughout its entire operating range, with a peak value of 97.39%. In contrast to the initial structure, the proposed design not only achieves a much broader frequency spectrum but also exhibits superior and more stable radiation performance. This confirms that the integration of cascaded elliptical slots and concentric arc parasitic patches effectively facilitates energy radiation without introducing significant ohmic losses, supporting the high-performance claims summarized in Table 2.

Furthermore, the time-domain performance of the proposed PA is investigated to ensure its reliability in impulse-based UWB sensing and imaging. As shown in Fig. 9(a), the group delay remains remarkably stable across the operating band, indicating excellent phase linearity and minimal signal dispersion. This is further corroborated by the normalized impulse response in Fig. 9(b), which exhibits a sharp, concentrated pulse with negligible ringing. To quantitatively evaluate signal integrity, the system fidelity factor (SFF) is determined by calculating the maximum value of the normalized cross-correlation between the input Gaussian doublet and the received pulse. As illustrated in Fig. 9(c), the received waveform follows the reference pulse closely with a high SFF value of 0.93, confirming that the pulse shape is preserved with high fidelity. This superior time-domain performance, combined with its wide bandwidth and compact footprint, makes the antenna highly competitive for high-resolution applications.

TABLE 3. Performances of the PA and reference antennas.

Ref.	Size (mm^3)	Operational Bandwidth (GHz)	ε_r
[3]	$34 \times 33 \times 0.8$	3.2–16.8	4.4
[4]	$40 \times 40 \times 1$	1.59–5.51	2.65
[5]	$31 \times 20 \times 0.51$	5–40	2.2
[6]	$158 \times 125 \times 1$	0.72–17	2.55
[7]	$38.5 \times 25 \times 1.6$	2.82–12.9	4.4
[8]	$180 \times 125.1 \times 20$	0.78–20	3.3
[10]	$177 \times 127 \times 1.57$	0.36–15	2.2
This Work	$14.5 \times 19.8 \times 0.51$	6.61–21.06	3.66

Table 3 compares the physical dimensions and operating bandwidth of the presented PA with those of various recently reported Vivaldi antennas. Different design strategies have been adopted to balance antenna miniaturization and broadband performance. Some existing designs achieve an ultra-wide impedance bandwidth at the expense of increased antenna size or substrate thickness, whereas other compact structures realize a certain degree of miniaturization but suffer from limited operating bandwidth. Notably, compared with the recently reported Vivaldi antenna [3], which utilizes inclined slots and occupies an area of 1122 mm^2, the presented PA achieves a similar lower-frequency coverage in a compact footprint of only 287.1 mm^2. This represents a significant area reduction of approximately 74.4%. By synergistically integrating cascaded overlapping slots and concentric arc patches, the presented antenna breaks the trade-off between extreme miniaturization and ultra-wide bandwidth, achieving a relative bandwidth of 104.45% while strictly maintaining a simple single-layer planar structure.

In contrast, the presented PA achieves a wide impedance bandwidth of 6.61–21.06 GHz while maintaining a single-layer planar configuration, with a compact physical size of only $14.5 \times 19.8 \times 0.51\,mm^3$, which is among the smallest listed in Table 3 under comparable substrate thickness and dielectric constant conditions. The presented antenna preserves excellent UWB performance while significantly reducing the an-

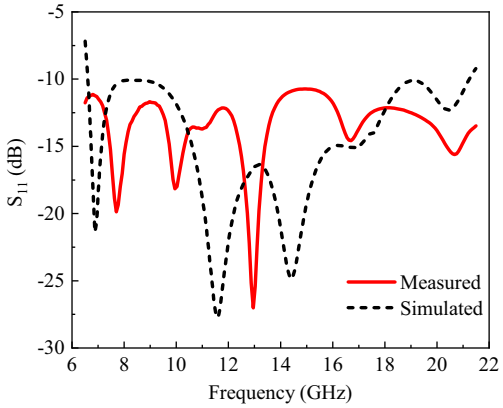

FIGURE 11. Simulated and measured reflection coefficients (S_{11}) of the PA.

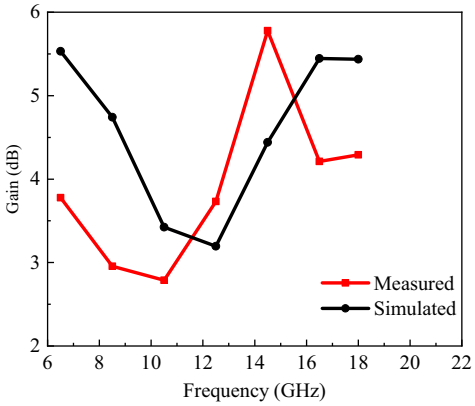

FIGURE 12. Simulated and measured gains of the PA.

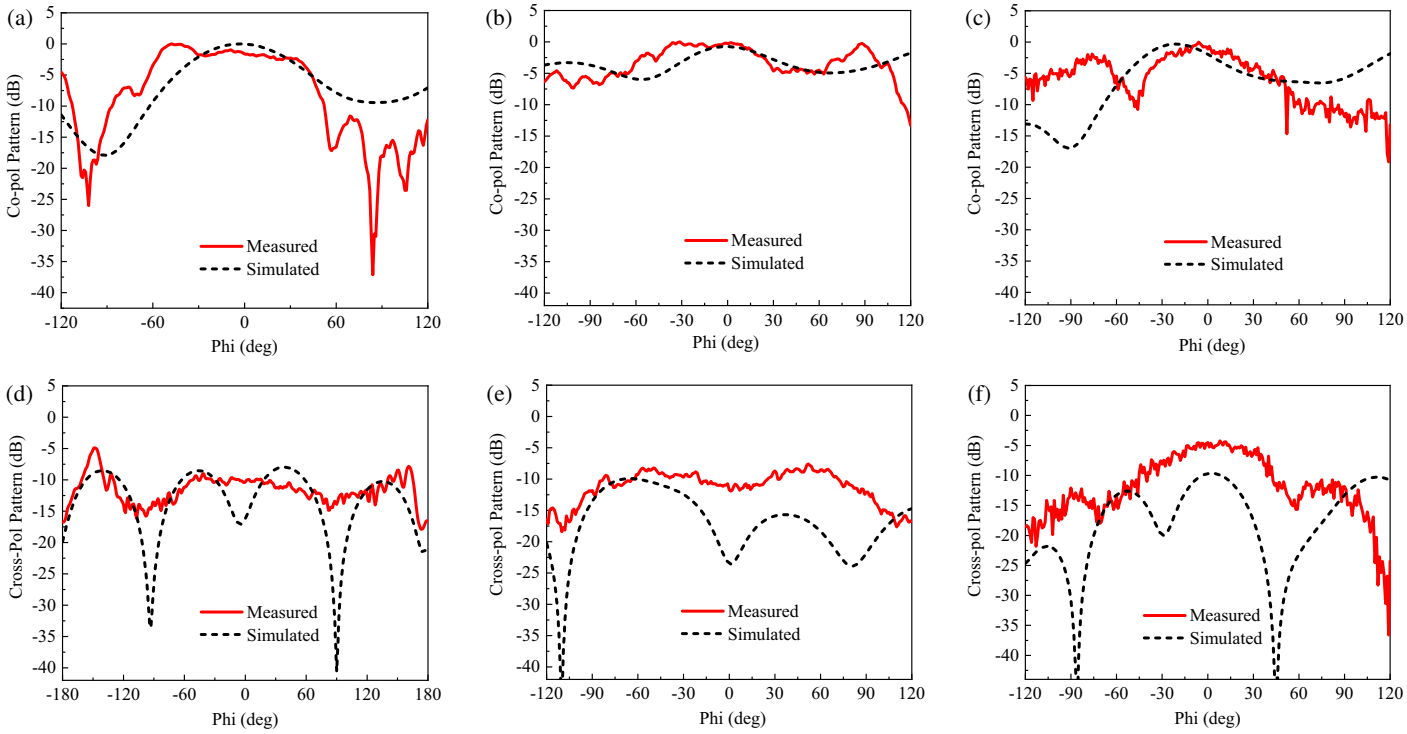

FIGURE 13. Simulation and measurement comparison of normalized radiation patterns of the PA antenna at different frequencies. (a) Co-pol at 8.5 GHz. (b) Cross-pol at 8.5 GHz. (c) Co-pol at 12.5 GHz. (d) Cross-pol at 12.5 GHz. (e) Co-pol at 18.0 GHz. (f) Cross-pol at 18.0 GHz.

tenna size, demonstrating a favorable trade-off between miniaturization and bandwidth. Moreover, the presented structure does not rely on complex approaches such as array configurations or periodic loading. Instead, broadband and miniaturized characteristics are simultaneously achieved through simple geometrical loading, which helps reduce the design complexity and fabrication cost, making the antenna well suited for compact UWB system integration.

3. RESULTS AND DISCUSSION

To verify the performance of the proposed antenna, a prototype was fabricated and tested. The reflection coefficient (S_{11}) was measured using an AV3672C-S vector network analyzer (VNA). To ensure measurement accuracy across the operating band, a standard Short-Open-Load-Thru (SOLT) calibration was performed from 6 GHz to 22 GHz prior to testing. The antenna was fed through a 1.6 mm offset-type SMA connector, which was precisely connected to the microstrip feedline via soldering. To eliminate the parasitic effects and phase shift introduced by the connector and the transition, a de-embedding process was applied during the measurement. Furthermore, the radiation characteristics were characterized in a microwave anechoic chamber to minimize environmental reflections. The measurement setup and the fabricated antenna are shown in Fig. 10.

Figures 11 and 12 present the comparisons between the simulated and measured reflection coefficients (S_{11}) and peak gains of the PA antenna. It can be observed that the measured

S_{11} remains below -10 dB over the frequency range of 6.61–21.06 GHz, while the measured peak gain follows the simulated trend with values ranging from 2.79 to 5.78 dBi across the 6.5–18.0 GHz band. Maximum measured gain of 5.78 dBi is achieved at 14.5 GHz, confirming that the presented antenna achieves both good ultra-wide impedance bandwidth and stable radiation capability. Both sets of measured curves exhibit good agreement with the simulated results in terms of the overall trend, while minor discrepancies are observed at certain frequency points. These differences are primarily attributed to fabrication tolerances (approximately ± 0.05 mm) and uncertainties in the substrate's relative permittivity. Additionally, the residual parasitic effects from the manual soldering of the 1.6 mm offset SMA connector, which were not fully captured in the simulation despite the de-embedding process, also contribute to the measured uncertainties in both S_{11} and gain. Overall, the experimental results confirm the reliability of the simulation analysis.

Figure 13 presents the simulated and measured normalized radiation patterns of the PA antenna at three representative frequencies of 8.5 GHz, 12.5 GHz, and 18.0 GHz, including both co-polarized and cross-polarized components. From the co-polarized patterns, it can be observed that the antenna maintains stable radiation characteristics at different operating frequencies, with consistent main-beam directions. The overall radiation patterns vary smoothly with frequency, exhibiting the typical end-fire radiation behavior of Vivaldi antennas. As the frequency increased, slight fluctuations were observed. However, the overall radiation performance remained consistent. From the cross-polarized patterns, it can be seen that the cross-polarization levels are generally lower than the co-polarization levels over the selected frequency range, and the measured results show trends that are in good agreement with the simulated ones. A slight increase in cross-polarization was observed at higher frequencies, which is mainly attributed to the higher-order mode excitation and finite-size effects of the antenna. This phenomenon is commonly observed in compact ultra-wideband (UWB) Vivaldi antennas.

Based on the above reflection coefficient and radiation performance results, it can be concluded that the proposed PA antenna achieves significant miniaturization while maintaining good UWB impedance matching and stable radiation characteristics. These results validated the feasibility of the proposed design for compact UWB system integration applications.

4. CONCLUSION

A novel compact UWB Vivaldi antenna is presented and experimentally validated in this study. By introducing cascaded elliptical slots into the radiating arms and loading concentric arc patches at the front end of the tapered slot, the surface current distribution can be effectively regulated without increasing the antenna layers or structural complexity. As a result, a significant size reduction was achieved while maintaining ultra-wide impedance bandwidth. Both simulated and measured results demonstrate that the presented antenna operates over 6.61–21.06 GHz with stable end-fire radiation characteristics and low cross-polarization levels at several representative frequencies. Compared with the recently reported Vivaldi antennas, the proposed design exhibits a favorable trade-off between miniaturization and UWB performance. This study provides a simple and cost-effective solution for a compact UWB Vivaldi antenna design with strong potential for practical engineering applications.

ACKNOWLEDGEMENT

This work was supported in part by the National Natural Science Foundation of China (NSFC) under Grant No. 62461054, Grant 62501519, and Grant 62361054, and in part by the Natural Science Basic Research Plan in Shaanxi Province of China under Grant 2025JC-YBMS-684.

REFERENCES

[1] Gibson, P. J., "The Vivaldi aerial," in *1979 9th European Microwave Conference*, 101–105, Brighton, UK, 1979.

[2] Hossain, A. and A.-V. Pham, "A novel gain-enhanced miniaturized and lightweight Vivaldi antenna," *IEEE Transactions on Antennas and Propagation*, Vol. 71, No. 12, 9431–9439, 2023.

[3] Zhang, H. and F. Zhang, "A novel ultrawideband miniature Vivaldi antenna with sawtooth outer edges and inclined elliptical slots," *IEEE Antennas and Wireless Propagation Letters*, Vol. 23, No. 9, 2708–2712, 2024.

[4] Liu, X., Y. Zhu, and W. Xie, "Miniaturized ultrawideband circularly polarized antenna with folded arms inspired by the conventional Vivaldi antenna," *IEEE Antennas and Wireless Propagation Letters*, Vol. 22, No. 12, 2768–2772, 2023.

[5] Yin, Z., G. He, X.-X. Yang, and S. Gao, "Miniaturized ultrawideband half-mode Vivaldi antenna based on mirror image theory," *IEEE Antennas and Wireless Propagation Letters*, Vol. 19, No. 4, 695–699, 2020.

[6] Honari, M. M., M. S. Ghaffarian, and R. Mirzavand, "Miniaturized antipodal Vivaldi antenna with improved bandwidth using exponential strip arms," *Electronics*, Vol. 10, No. 1, 83, 2021.

[7] Zhao, G., Y. Xiao, W. Huang, S. Xu, and Z. Chen, "Compact and gain-enhanced Vivaldi antenna design using nonuniform slot profile optimization and aperture dielectric loading," *IEEE Antennas and Wireless Propagation Letters*, Vol. 24, No. 7, 1570–1574, 2025.

[8] Wu, B., X.-Y. Sun, H.-R. Zu, H.-H. Zhang, and T. Su, "Transparent ultrawideband halved coplanar Vivaldi antenna with metal mesh film," *IEEE Antennas and Wireless Propagation Letters*, Vol. 21, No. 12, 2532–2536, 2022.

[9] Lalitha, K. and J. Manjula, "Design of UWB antipodal Vivaldi antenna with parasitic patch for microwave head imaging system," in *2022 International Conference on Computing, Communication, Security and Intelligent Systems (IC3SIS)*, 1–6, Kochi, India, 2022.

[10] Hossain, A., S. Wagner, S. Pancrazio, and A.-V. Pham, "An electrically highly compact ultra-wideband Vivaldi antenna with substantial gain performance," *IEEE Open Journal of Antennas and Propagation*, Vol. 6, No. 6, 1936–1947, 2025.

[11] Gupta, K., V. Anjitha, A. O. Asok, and S. Dey, "Design of an ultra-wideband antipodal Vivaldi antenna for deep ground penetration and high-resolution through-wall imaging," in *2025 IEEE Space, Aerospace and Defence Conference (SPACE)*, 1–5, Bangalore, India, 2025.

[12] Qin, Z., S. Cao, W. Li, and Q. Huang, "A miniaturized ultrawideband ground penetrating radar antenna based on the Vivaldi

structure," *Progress In Electromagnetics Research C*, Vol. 156, 141–146, 2025.

[13] Pisa, S., F. Pastori, R. Cicchetti, E. Piuzzi, O. Testa, E. Pittella, A. Cicchetti, P. D'Atanasio, and A. Zambotti, "An antipodal Vivaldi antenna for a drone-mounted ground probing radar," *Progress In Electromagnetics Research M*, Vol. 123, 53–61, 2024.

[14] Bhavani, M. V. L., D. Chaturvedi, T. Lanka, T. A. Raju, G. Rana, and A. Kumar, "A non-invasive microwave imaging system for breast tumor detection using a high gain Vivaldi antenna array sensor," *IEEE Sensors Journal*, Vol. 25, No. 17, 32 631–32 640, 2025.

[15] Zhao, L. L., A. D. Li, C. W. Li, Y. M. Wang, M. X. Zheng, D. Song, C. L. Liu, Y. Liang, H. Zhao, C. F. Hu, and T. Ma, "A miniaturized antipodal Vivaldi antenna for high-power design in X-band," *Progress In Electromagnetics Research M*, Vol. 129, 105–110, 2024.

[16] Birwal, A., K. Patel, and S. Singh, "A directional wide-band antipodal Vivaldi antenna for imaging applications," *Progress In Electromagnetics Research C*, Vol. 127, 227–237, 2022.

[17] Parveen, F. and P. Wahid, "Design of miniaturized antipodal Vivaldi antennas for wideband microwave imaging of the head," *Electronics*, Vol. 11, No. 14, 2258, 2022.

[18] Wang, B., H. Ning, H. Cai, Q. Liu, Y. Wang, and Y. Yan, "Pulse radiation characteristics prediction method of Vivaldi antenna based on dipole array," *Applied Computational Electromagnetics Society Journal (ACES)*, Vol. 39, No. 5, 422–432, 2024.